

https://doi.org/10.1070/QEL17059

Effect of recovery time of nonlinear absorber saturated losses on the soliton pulse structure in a fibre laser with different cavity lengths

A.A. Mastin, P.A. Ryabochkina

Abstract. **Using numerical simulation methods, we have calculated the dependences of the pulse profile and spectrum of a ring fibre laser in the region of anomalous group velocity dispersion on the length of the laser cavity and the recovery time of the nonlinear absorber saturated losses. It is found that with increasing cavity length the laser pulse acquires a pedestal, the positions of its edges corresponding to the frequencies of the Kelly sidebands. It is shown that the finiteness of the recovery time of the saturable absorber leads to an asymmetry in the profile and spectrum of the laser pulse.**

Keywords: *soliton fibre laser, Kelly sidebands, saturable losses, nonlinear saturable absorber, recovery time.*

1. Introduction

Interest in fibre soliton lasers is due to the possibility of generating subpicosecond pulses directly in the laser cavity without using external compression [1–6]. The formation of such pulses occurs due to the anomalous group velocity dispersion and self-phase modulation. The spectrum of a soliton-like pulse has a Gaussian profile with characteristic Kelly sidebands [7, 8]. The latter are formed because of interference amplification of the spectral components of the pulse, which due to the phase velocity dispersion acquire during the cavity roundtrip a phase incursion multiple of 2π, relative to the phase of the carrier frequency spectral component of the pulse [7–9].

The pulsed laser operation can be implemented using a nonlinear saturable absorber, which allows passive mode locking. SESAM semiconductor structures and structures based on carbon nanotubes are widely used as such absorbers [3–6]. The absorber produces losses saturated by the laser pulse intensity, which are restored depending on its recovery time that is an important characteristic determining the maximum permissible pulse energy [9–12]. The recovery time of a nonlinear absorber can be several times longer than the pulse duration [10–12]. The finiteness of the absorber recovery time significantly affects the leading edge of the pulse, practically does not affect its trailing edge [10] and, in fact, is a destabilising factor leading to an increase in instabilities after the pulse, where the selective action of the absorber is absent and the gain of the active medium is preserved. This leads to an increase in noise and destabilisation of the laser pulse [10–12].

It should be noted that at present there are no detailed data on the effect of the recovery time of saturable absorber losses on the pulse profile and spectrum in a fibre laser with different cavity lengths. In this connection, the aim of this work was to study by means of numerical simulation the influence of the recovery time of the saturated state of the absorber on the pulse profile and spectrum in a fibre laser with different cavity lengths in the region of anomalous group velocity dispersion.

A.A. Mastin Technopark-Mordovia, ul. Lodygina 3, 430034 Saransk, Russia; e-mail: mastinaa@mail.ru;
P.A. Ryabochkina Ogarev Mordovia State University, ul. Bol'shevistskaya 68, 430005 Saransk, Russia; e-mail: ryabochkina@freemail.mrsu.ru

Received 9 May 2019; revision received 11 June 2019
Kvantovaya Elektronika **49** (9) 819–823 (2019)
Translated by V.L. Derbov

2. Description of the numerical model

In the general case, the dynamics of the pulse in the active fibre of the laser cavity is described by the nonlinear Schrödinger equation in the frequency representation [13]:

$$\frac{\mathrm{d}U(z,\omega)}{\mathrm{d}z} = \mathrm{i}\sum\beta_n\omega^n U(z,\omega) + \mathrm{i}\gamma G(z,\omega) + \left(1-\frac{\omega^2}{\Omega^2}\right)g(z)\,U(z,\omega), \quad (1)$$

where ω is the frequency detuning of the laser pulse from the carrier frequency ω_0; z is the coordinate along the cavity of the fibre laser; $U(\omega,z)=\int_{-\infty}^{\infty}\tilde{U}(z,t)\exp(-\mathrm{i}\omega t)\,\mathrm{d}t$ is the spectral amplitude of the pulse field; $\tilde{U}(z,t)$ is the slowly varying amplitude of the pulse field; $G(\omega,z)=\int_{-\infty}^{\infty}|\tilde{U}(z,t)|^2\tilde{U}(z,t)\exp(-\mathrm{i}\omega t)\,\mathrm{d}t$ is the Fourier transform of the self-phase modulation function of the pulse field; β_n is the group velocity dispersion of the pulse; γ is the Kerr nonlinearity coefficient of the medium; and Ω is the half-width of the parabolic-shaped gain line of the active medium.

Due to the group velocity dispersion and self-phase modulation, the instantaneous frequency is not constant during the pulse. The distribution of frequency (wavelength) over the pulse duration (chirp) can be obtained from the expression

$$\omega(z,t)_{\mathrm{ch}} = \frac{\partial}{\partial t}\left(\arctan\frac{\mathrm{Im}(\tilde{U}(z,t))}{\mathrm{Re}(\tilde{U}(z,t))}\right). \quad (2)$$

The pulse wavelength at time t is expressed as

$$\lambda(z,t)_{\mathrm{ch}} = \frac{2\pi c}{\omega(z,t)_{\mathrm{ch}}+\omega_0}. \quad (3)$$

The saturation of the active medium is determined by the relation

$$g(z) = \frac{g_0}{1 + E_p/(P_g T_R)}, \quad (4)$$

where g_0 is the small-signal gain; P_g is the gain saturation power of the active medium; and T_R is the cavity round-trip time of the pulse. The pulse energy and signal power, respectively, have the form

$$E_p(z) = \int P(z,t)\,dt, \quad (5)$$

$$P(z,t) = |\tilde{U}(z,t)|^2. \quad (6)$$

The dynamics of saturable losses of a passive nonlinear absorber is described by the equation

$$\frac{\partial q(t)}{\partial t} = -\frac{q(t) - q_0}{\tau_a} - \frac{q(t)\,|\tilde{U}(z,t)|^2}{\tau_a P_a}, \quad (7)$$

where $q(t)$ is the coefficient of signal absorption by the absorber; q_0 is the absorption coefficient for a weak signal; τ_a is the recovery time of the saturated state of the absorber; and P_a is the saturation power of the losses introduced by the nonlinear absorber.

For a fast absorber, the condition $\tau_a \ll T_p$ holds, where T_p is the pulse duration. Then

$$q(t) = \frac{q_0}{1 + |\tilde{U}(z,t)|^2/P_a}. \quad (8)$$

In this case, the amplitude $\tilde{U}_2(z,t)$ of the pulse transmitted through the absorber can be presented in the form

$$\tilde{U}_2(z,t) = F\tilde{U}_1(z,t),$$

where $\tilde{U}_1(z,t)$ is the input signal; and F is the pulse transfer function of the absorber:

$$F = 1 - q(t). \quad (9)$$

The structure of the fibre laser pulse was calculated numerically by solving Eqn (1) with the ode45 computational procedure of the Matlab software. The search for a solution was carried out in the process of multiple passage of the pulse through the cavity. The optimal solution was chosen according to the condition of pulse profile stabilisation. As a rule, to obtain the optimal solution, 100–150 pulse passes through the cavity were required.

In this work, the simulation was carried out for a two-micron ring fibre laser, the active medium of which was a silica fibre doped with Tm^{3+} ions. The laser is schematically shown in Fig. 1. The ring fibre laser incorporates a multiplexer (*1*) for delivering the pump, an active fibre (*2*) having the length L_1, a power divider (*3*), a passive nonlinear absorber (*4*), and a passive fibre (*5*) having the length L_2. In the simulation, the frequency filtering properties of the cavity components were not taken into account. It was assumed that the pulse in the laser cavity propagates clockwise and that 90% of the pulse energy is extracted from the cavity using a power divider [14–16].

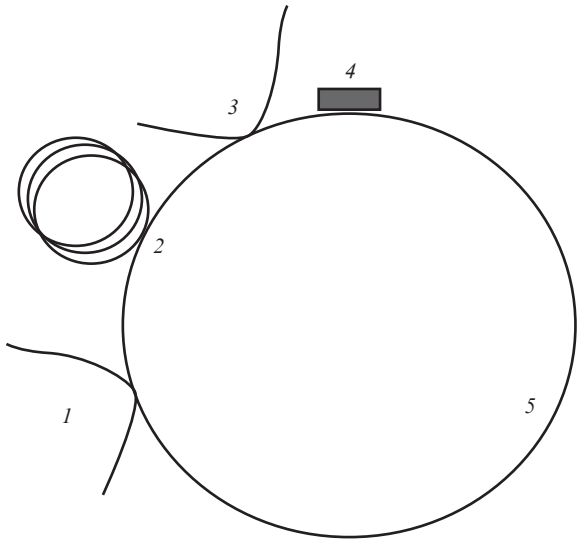

Figure 1. Schematic of the ring fibre laser used to model the structure of a soliton pulse.

The pulse structure was simulated for four configurations of the fibre laser cavity:

1) a short-cavity laser (passive fibre length $L_2 = 0.5$ m) and a saturable absorber with an infinitely short time of absorption recovery ($\tau_a = 0$, 'fast' absorber);

2) a short-cavity laser ($L_2 = 0.5$ m) and a saturable absorber with finite absorption recovery time ($\tau_a = 8$ ps, 'slow' absorber);

3) a long-cavity laser ($L_2 = 5$ m) and a saturable absorber with $\tau_a = 0$; and

4) a long-cavity laser ($L_2 = 5$ m) and a saturable absorber with $\tau_a = 8$ ps.

Below in the text, the lasers with the cavity configurations 1, 2, 3, 4 will be referred to as lasers 1, 2, 3, 4, respectively.

Below we present the values of the cavity parameters of a ring fibre laser, which were used to simulate the pulse structure. The simulation was performed using the gain g_0 corresponding to a pulse with maximum energy in a single-pulse regime for the period of the cavity round-trip.

Group velocity dispersion, β_2/ps^2 m^{-1}	−0.0695
Third-order group velocity dispersions, β_3 /ps^3 m^{-1}	0.0003
Fibre nonlinearity coefficient, γ/W^{-1} m^{-1}	0.0012
Gain saturation power of the active fibre, P_g/W	.0.02
Active fibre length, L_1/m	0.3
Small-signal absorption coefficient, q_0	0.3
Loss-saturation power of the nonlinear absorber, P_a/W	10
Half-width of the active medium gain line, Ω/ps^{-1}	2.7

3. Simulation results and discussion

As a result of the simulation, the power profiles $P(z, t)$ and the spectra of laser pulses $U(\omega, z)$ emerging from the cavity through the power divider were calculated. In the process of modelling, it was assumed that the pulse energy corresponds to the maximum possible one under the condition of the single-pulse generation regime.

The power profiles (6) and transmission functions of the nonlinear absorber (9) obtained by the simulation for fibre lasers 1 and 2 are shown in Fig. 2. It is seen that the absorber

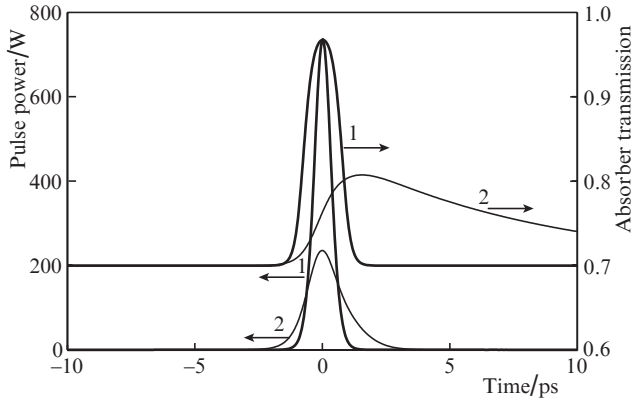

Figure 2. Pulse power profiles and absorber transmission function for lasers 1 and 2.

with a finite recovery time is characterised by the presence of a section with small losses after the passage of the pulse. This leads to the appearance of an asymmetry in the pulse profile; its trailing edge becomes gentler than the leading one.

The following values of the pulse energy were calculated with the gain of the active fibre $g_0 = 22$ m^{-1} for lasers 1 and 2: the pulse energy after the power divider $E_{1p} = 0.62$ nJ (laser 1) and 0.42 nJ (laser 2), and the energy of the pulse entering the absorber $E_{2p} = 0.07$ nJ (laser 1) and 0.05 nJ (laser 2).

Note that with the same gain g_0, the pulse energy of the laser with a 'slow' absorber is lower than that of the laser with a 'fast' absorber. Therefore, an increase in the absorption recovery time leads to a decrease in the pulse energy.

Figure 3 shows on a logarithmic scale the profiles of the pulses of fibre lasers 1 and 2 normalised to the maximum value and the corresponding chirps. It can be seen from the figure that the laser 1 pulse chirp has a symmetrical step shape, and the leading edge of the pulse is characterised by shorter wavelengths of the chirp than the trailing edge. The finite recovery time of the saturable absorber in laser 2 leads to the asymmetry and shift of its pulse chirp to the long-wavelength region relative to the pulse chirp of laser 1.

The lasing spectra for lasers 1 and 2 normalised to the maximum value are shown on a logarithmic scale in Fig. 4. The finite recovery time of the saturable absorber in laser 2 leads to a shift in the spectrum of the laser pulse generation towards the long-wavelength region relative to the spectrum of the pulse of laser 1. The latter can be explained by the influence of the 'slow' absorber on the leading edge of the pulse, which is characterised by shorter wavelengths of the chirp than the trailing edge (see Fig. 3). The finite recovery time of the saturable absorber leads to greater losses at the leading edge of the pulse than at the trailing edge (see Fig. 2). In turn, this leads to a redistribution of energy over the pulse profile, as evidenced by a decrease in the area under the pulse profile curve in the chirp short-wavelength region and its increase in the long-wavelength region, and, ultimately, to a shift in the pulse spectrum of laser 2 to longer wavelengths.

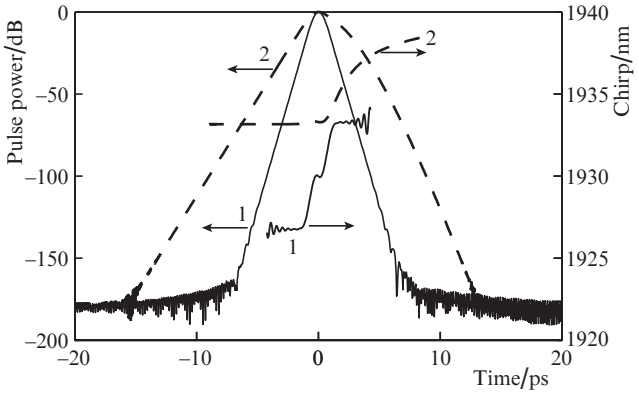

Figure 3. Power profiles and pulse chirps of lasers 1 and 2.

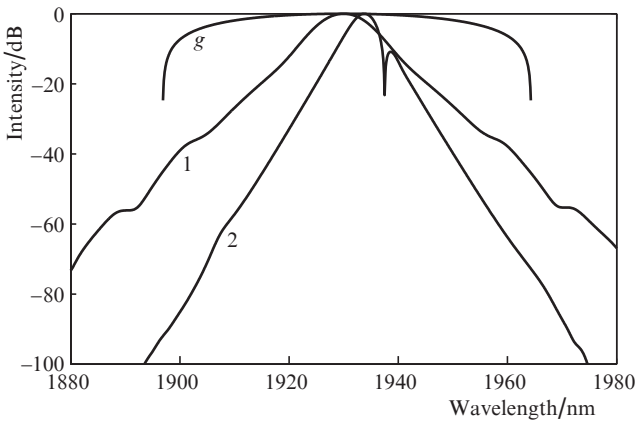

Figure 4. Spectra of the generation pulses of fibre lasers 1 and 2, as well as the spectral gain profile of the active medium g.

Figure 5 shows the calculated power profiles of the laser pulse and the transmission function of a nonlinear absorber for lasers 3 and 4. Note that the transmission function of the saturable absorber of laser 3 is characterised by the presence of oscillations that arise due to the influence of low-intensity pulse edges on the absorber.

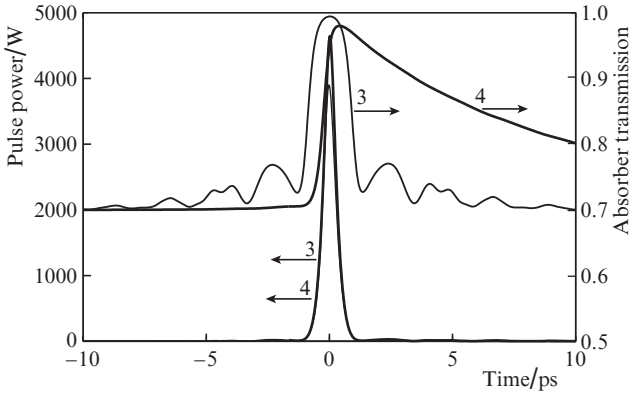

Figure 5. Pulse power profiles and transmission functions of a saturable absorber for lasers 3 and 4.

The following values of pulse energy were calculated for lasers 3 and 4 (laser pulse energy of 3 and 4 nJ, respectively) with the active fibre gain $g_0 = 16$ m^{-1}: the pulse energy after the power divider $E_{1p} = 3.57$ nJ (laser 3) and 3.48 nJ (laser 4); the energy of the pulse entering the absorber $E_{2p} = 0.40$ nJ (laser 3) and 0.39 nJ (laser 4).

Figure 6 shows on a logarithmic scale the profiles of the pulse power normalised to the maximum value and the cor-

responding chirps for lasers 3 and 4. The pulse power profiles of these lasers are characterised by a central peak and a low-intensity wide pedestal with an oscillating profile. A similar structure of the pulse observed in the study of bound states of pulses in a soliton laser was described in Ref. [11]. Such a pedestal is not typical for lasers 1 and 2 (see Fig. 3). The appearance of a pedestal on the profile of pulses of lasers 3 and 4 is apparently associated with an increase in the dispersion of the cavities of these lasers compared to lasers 1 and 2.

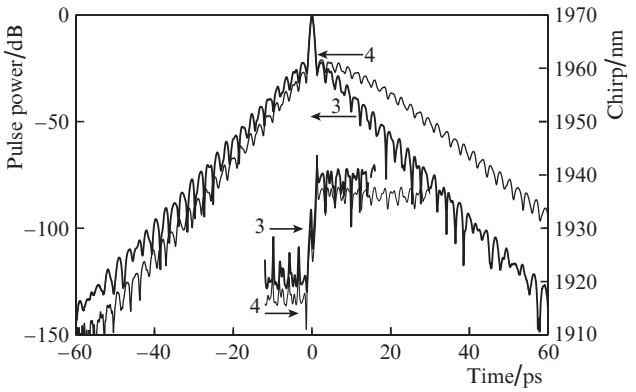

Figure 6. Pulse power profiles and chirps of lasers 3 and 4.

The chirp of pulses in lasers 3 and 4 has a step profile with oscillations. The comparison of the chirp and the pulse profile shows that the wavelength of the leading edge of the pulse pedestal is smaller than the wavelength of the central peak. In this case, the trailing edge of the pedestal is characterised by a longer wavelength of the chirp compared to the central peak. The central peak of the pulse has a positive chirp, characteristic of a soliton-like pulse with anomalous group velocity dispersion.

The pulse intensity spectra of lasers 3 and 4 normalised to the maximum intensity are shown in Fig. 7 on a logarithmic scale. It is seen that the presence of Kelly sidebands is characteristic of these spectra. The wavelengths of the first Kelly peaks in the spectra of lasers 3 and 4 coincide with the wavelengths of the chirp of the leading and trailing edges of the pedestal of the corresponding pulses (see Fig. 6). For laser 3, the wavelengths of the first Kelly peaks are 1920 and 1940 nm.

An increase in the cavity length in lasers 3 and 4 led to a decrease in the separation between the carrier wavelength of the pulse and the wavelengths of the Kelly sidebands, because of which they appeared to be within the gain band of the active medium. These spectral components were amplified and formed the pulse pedestals of lasers 3 and 4. The wavelengths of the Kelly sidebands for lasers 1 and 2 were outside the gain band due to the shorter length of their cavities, and so the pulse pedestal was not formed.

The chirp structure of the pulses of lasers 3 and 4 leads to instability of the pedestal shape during the free propagation of the pulse in the fibre. Due to the anomalous dispersion of the group velocity, the leading edge of the pulse pedestal is ahead of the central peak, and the trailing edge is behind it. The stability of the pulse pedestal shape is determined by the action of saturable absorber. The saturable absorber periodically corrects the shape of a pedestal spreading in time due to dispersion.

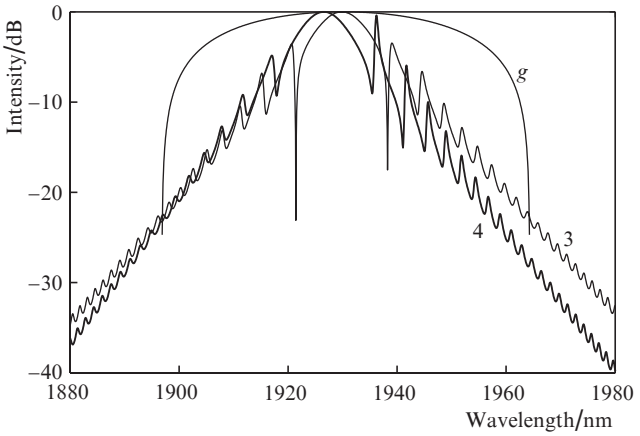

Figure 7. Pulse spectra of lasers 3 and 4, as well as the spectral gain profile of the active medium g.

In laser 3 with a 'fast' absorber, the pulse profile is symmetrical (see Fig. 6). The finite recovery time of the absorber losses in fibre laser 4 leads to the asymmetry of the pulse profile, which ensures the redistribution of the energy of the pedestal over the pulse profile. The area under the curve of the pedestal in the chirp short-wavelength region decreases, and in the region of the long waves of the chirp it increases. In laser 4, in contrast to laser 3, the Kelly sideband intensities are redistributed. It can be seen from Fig. 7 that, for laser 4, the intensity of the first short-wavelength Kelly peak decreases, while the first long-wavelength peak increases. This redistribution of the intensities of the Kelly peaks correlates with the rearrangement of the shape of the pedestal of the pulse profile (see Fig. 6). The change in the areas under the pulse pedestal fronts corresponding to the short-wavelength and long-wavelength sections of the chirp is consistent with changes in the intensities of the corresponding Kelly peaks.

The finite recovery time of the saturable absorber in laser 4 provides a shift of the spectrum of the laser pulse to the short-wavelength region (see Fig. 7), while in laser 2 the pulse spectrum shifts to the long-wavelength region (see Fig. 4).

The short-wavelength shift of the pulse spectrum of laser 4 can be explained by the asymmetric arrangement of the central peak on the pulse pedestal. Due to the finite recovery time of the saturable absorber losses, the central peak of the laser pulse is shifted to the short-wavelength region of the pedestal, which leads to a shift in the entire spectrum.

4. Conclusions

A numerical simulation was used to study the effect of the recovery time of the losses of a nonlinear absorber on the profile and pulse spectrum of a thulium-doped fibre laser with different cavity lengths in the region of anomalous group velocity dispersion. It is shown that an increase in the total dispersion of the cavity leads to the appearance of a low-intensity wide pedestal on the pulse profile.

The chirp of a soliton-like pulse of the fibre laser has a step profile. The positions of the leading and trailing edges of the pedestal of the fibre laser pulse correspond to the wavelengths of the Kelly sidebands.

The finite recovery time of the losses in the absorber leads to redistribution of the pulse pedestal energy relative to the central peak, as evidenced by a decrease in the area under the pulse profile with short wavelengths of the chirp and an

increase in the area under the pulse profile with longer wavelengths. The influence of the finiteness of the saturated absorber recovery time on the laser pulse spectrum is determined by the presence of a pedestal on the pulse profile. In the absence of a pedestal, the finiteness of the recovery time leads to a shift of the laser pulse spectrum to the long-wavelength region, and in the presence of a pedestal, to a shift of the spectrum to the short-wavelength side.

The results obtained during the simulation can be of interest in the development of fibre soliton lasers.

Acknowledgements. This work was supported by the Russian Foundation for Basic Research (Grant No. 18-42-130001 R_a).

References

1. Mitschke F.M., Mollenauer L.F. *Opt. Lett.*, **12**, 407 (1987).
2. Kafka J.D., Baer T., Hall D.W. *Opt. Lett*., **14**, 1269 (1989).
3. Solodyankin M.A., Obraztsova E.D., Lobach A.S., Chernov A.I., Tausenev A.V., Konov V.I., Dianov E.M. *Opt. Lett*., **33**, 1336 (2008).
4. Rahman M.F.A., Latiff A.A., Rosol A.H.A. *J. Lightwave Technol*., **36**, 3522 (2018).
5. Yarutkina I.A., Shtyrina O.V. *Quantum Electron*., **43**, 1019 (2013) [*Kvantovaya Elektron*., **43**, 1019 (2013)].
6. Ahmad H., Reduan S.A., Ismail M.F., Thambiratnam K. *Quantum Electron*., **48**, 930 (2018) [*Kvantovaya Elektron*., **48**, 930 (2018)].
7. Kelly S.M.J. *Electron. Lett*., **28**, 806 (1992).
8. Dennis M.L., Duling I.N. *IEEE J. Quantum Electron*., **30**, 1469 (1994).
9. Tang D., Fleming S., Man W., Tam H., Demokan M. *J. Opt. Soc. Am. B*, **18**, 1443 (2001).
10. Paschotta R., Keller U. *Appl. Phys. B*, **73**, 653 (2001).
11. Zolotovskii I.O., Korobko D.A., Gumenyuk R.V., Okhotnikov O.G. *Quantum Electron*., **45**, 26 (2015) [*Kvantovaya Elektron.*, **45**, 26 (2015)].
12. Jung D., Kärtner F.X., Brovelli L.R., Kamp M., Keller U. *Opt. Lett*., **20**, 1892 (1995).
13. Okhotnikov O.G. *Fiber Lasers* (Weinheim, Germany: Wiley, 2012).
14. Yang L., Wan P., Protopopov V., Liu J. *Opt. Express*, **20**, 5683 (2012).
15. Huang C. et al. *Sci. Rep.*, **5**, 13680 (2015).
16. Ortaç B., Limpert J., Tünnermann A. *Opt. Lett*., **32**, 2149 (2007).